24th INTERNATIONAL CONGRESS ON SOUND AND VIBRATION
23–27 July 2017, London

ICSV24
23-27JULY 2017
LONDON CALLING

EVALUATION OF DIFFERENT METHODS IN COMPUTATIONAL AEROACOUSTICS FOR NOISE PREDICTION AND MINIMIZATION OF A ROD-AIRFOIL CONFIGURATION

Beckett Y. Zhou, Tim Albring and Nicolas R. Gauger
Chair for Scientific Computing, TU Kaiserslautern, Germany
email: yuxiang.zhou@scicomp.uni-kl.de

Carlos R. Ilario da Silva, Thomas D. Economon, and Juan J. Alonso
Department of Aeronautics and Astronautics, Stanford University, USA

This paper aims to investigate the applicability of different computational aeroacoustics strategies for the prediction and henceforth reduction of noise generated by the flow interacting with airframe components. We apply both unsteady RANS and DES simulations coupled with a FW-H integral technique that are implemented in the SU2 multi-physics solver suite [1]. The rod-airfoil geometry has been chosen as the benchmark case and results of both flow field profiles and far-field noise spectra are presented. Results show good agreement with experimental data. In addition, coupled URANS-FWH and DES-FWH design sensitivities for noise minimization are developed based on a discrete-adjoint framework. Their efficacies in performing noise-minimized designs are also evaluated in this paper.

Keywords: adjoint, noise reduction, aeroacoustics

1. Introduction

For the design of next-generation aircraft that comply with ever more stringent noise regulations, efficient and robust simulation and design tools well-suited for unsteady aerodynamic and aeroacoustic problems are urgently needed. The development of such computational tools faces a number of unique challenges. Fine geometric details of a design can modify the nearfield acoustic source which in turn alters the farfield noise signature significantly – this has been observed in noise reduction studies at component-level such as landing gears and flap side-edges. The need to parameterize designs with fine geometric details inevitably leads to a large number of design variables which must be handled efficiently by any design tool. To that end, adjoint-based method [2] is a good method of choice due to the fact that the computational cost of the design sensitivities is independent of the number of design variables.

To date, a number of studies have been published on adjoint-based aeroacoustic optimization [3, 4, 5], most of which are based on 2D or 3D unsteady RANS (URANS) simulations for the near-field acoustic sources and integral methods, such as the Kirchhoff method or Ffwocs Williams-Hawkings (FW-H) analogy for the far-field noise propagation. URANS-based simulations, while computationally inexpensive compared to scale-resolving simulations such as LES and DNS, have been shown to be incapable of accurately capturing the salient features of many separated flows [6]. In addition, URANS computations are not able to predict the broadband noise component as they do not resolve the relevant turbulent scales. However, for aircraft design problems at realistic Reynolds numbers

($Re > 10^6$), due to the exceedingly high resolution requirement in the boundary layer, LES and DNS remain predominantly research tools and will not likely see widespread industry use before the year 2070 [7]. Adjoint-based noise minimizations with LES/DNS-based solvers are rare in the literature and mostly restricted to simple geometries.

Hybrid RANS-LES methods such as detached eddy simulation (DES) [8] or delayed detached eddy simulation (DDES) offer a good compromise between resolution and computational cost by modelling the attached boundary layer with RANS and resolving separated flow regions with LES. Precisely because of this element of empiricism involved in the DES-based approach, its accuracy must be carefully assessed through validation against experimental data. To that end, the rod-airfoil configuration, which consists of a symmetric airfoil placed downstream of a circular cylinder in sub-critical flow regime, is a particularly well-suited benchmark test case, as its far-field noise spectra exhibit both a pronounced tonal component from the periodic vortex shedding of the cylinder and a broadband component due to the turbulent wake impingement on the airfoil leading edge.

The goal of this paper is twofold: i) To validate, against experimental data obtained by Jacob et al. [9], the coupled DDES-FWH noise prediction approach implemented in the SU2 solver and compare against acoustic results obtained from 3D URANS computations, and ii) To validate the design sensitivities with respect to far-field noise objective function computed based on a discrete adjoint framework, thus paving the way to aeroacoustic optimization using high-fidelity simulations in the near future.

2. Overview of the Noise Prediction and Minimization Framework in SU2

2.1 DDES-FWH Noise Prediction Framework

The Stanford University Unstructured (SU2) open source software suite was specifically developed for solving problems governed by partial differential equations (PDEs) and PDE-constraned optimization problems. It was developed with the aerodynamic shape optimization problems in mind. Therefore the suite is centered around a second-order finite volume RANS solver capable of simulating compressible, turbulent flows commonly found in problems in aerospace engineering. The turbulence can be either modeled by the Spalart-Allmaras(S-A) model or the Menter Shear Stress Transport (SST) Model. For unsteady flows, a dual time-stepping method can be used to obtain time-accurate solutions. Recently, Molina et al. [10] extended the existing RANS framework based on the S-A turbulence model to enable DDES computations. In particular, a subgrid length scale based on vorticity alignment and a hybrid upwind/centered flux scheme tailored for DDES were implemented.

In the current work, in order to predict the far-field noise from the near-field flow variables computed by DDES, a permeable surface formulation of the FW-H analogy [11] was implemented in time domain. The computationally expensive quadrupole sources are neglected.

2.2 Unsteady Discrete Adjoint Framework

Assuming second-order dual time stepping is used for time integration, the discrete optimization problem can then be posed as:

$$\min_{\alpha} \quad J = f(U^{N_*}, \ldots, U^N, \alpha) \tag{1}$$

$$\text{subject to} \quad U^n = G^n(U^n, U^{n-1}, U^{n-2}, \alpha), \qquad n = 1, \ldots, N \tag{2}$$

where U is the spatially discretized state vector, G^n is a fixed-point iterator representing one time step in the forward integration, α is the vector of design variables and the noise objective function J is evaluated between $N_* \leq n \leq N$. One can express the Lagrangian associated with the above

constrained optimization problem as follows:

$$L = f(U^{N_*}, \ldots, U^N, \alpha) - \sum_{n=1}^{N} [(\bar{U}^n)^T (U^n - G^n(U^n, U^{n-1}, U^{n-2}, \alpha))] \tag{3}$$

where $\bar{U}^n$ is the adjoint state vector at time level n. From (3), the unsteady discrete adjoint equations can be derived in the fixed point form as:

$$\bar{U}^n_{i+1} = \left(\frac{\partial G^n}{\partial U^n}\right)^T \bar{U}^n_i + \left(\frac{\partial G^{n+1}}{\partial U^n}\right)^T \bar{U}^{n+1} + \left(\frac{\partial G^{n+2}}{\partial U^n}\right)^T \bar{U}^{n+2} + \left(\frac{\partial f}{\partial U^n}\right)^T, \; n = N, \ldots, 1 \tag{4}$$

where $\bar{U}^{n+1}$ and $\bar{U}^{n+2}$ are converged adjoint state vectors at time levels $n+1$ and $n+2$. The unsteady adjoint equations above are solved backward in time. At each time level n we iterate through inner iteration i until we have converged to $\bar{U}^n$. The highlighted terms here are evaluated by algorithmic differentiation (AD) in reverse mode at each iteration. To do so, reverse accumulation is performed at the beginning of each time level n to store the computational graph by evaluating G using converged state solution U_n. Then each inner iteration i proceeds by re-evaulating the tape using the updated adjoint vector $\bar{U}^n_i$, giving the highlighted terms. This continues within each time level n until the adjoint vector has converged to $\bar{U}^n$. Note that $\frac{\partial f}{\partial U^n} = 0$ for $n < N_*$. The sensitivity gradient can then be computed from the adjoint solutions:

$$\frac{dL}{d\alpha} = \frac{\partial f}{\partial \alpha} + \sum_{n=1}^{N} \left((\bar{U}^n)^T \frac{\partial G^n}{\partial \alpha} \right) \tag{5}$$

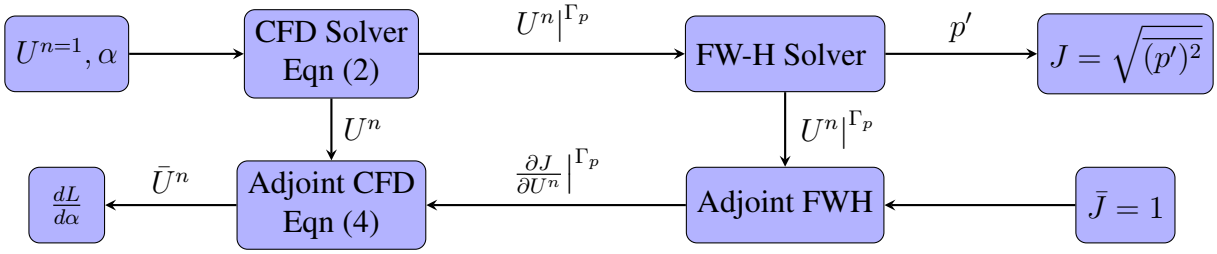

Figure 1: Computational chain of the coupled CFD-FWH noise prediction and optimization framework

The computational chain for the coupled CFD-FWH noise prediction and noise-adjoint framework is outlined on Figure 1. In the primal phase, unsteady flow field U^n is realized at each time step n by the DDES/URANS solver in SU2. $U^n|^{\Gamma_p}$ denotes the conservative flow variables at time step n extracted from the FW-H surface Γ_p which are then passed to the FW-H solver for far-field noise computation. In the adjoint phase, $\frac{\partial J}{\partial U^n}|^{\Gamma_p}$ denotes the sensitivity of the noise objective with respect to conservative flow variables evaluated Γ_p by the adjoint FW-H solver using $U^n|^{\Gamma_p}$, which is accumulated to the fixed-point iteration for the adjoint flow variables $\bar{U}^n$ in the adjoint CFD solver.

3. Results

3.1 Numerical Set-up for the Rod-Airfoil Configuration

The setup of the computational domain used in this test case is follows closely from the work of Giret et al. [15]. The domain extends 13C in the streamwise, 6C in the cross-stream direction and

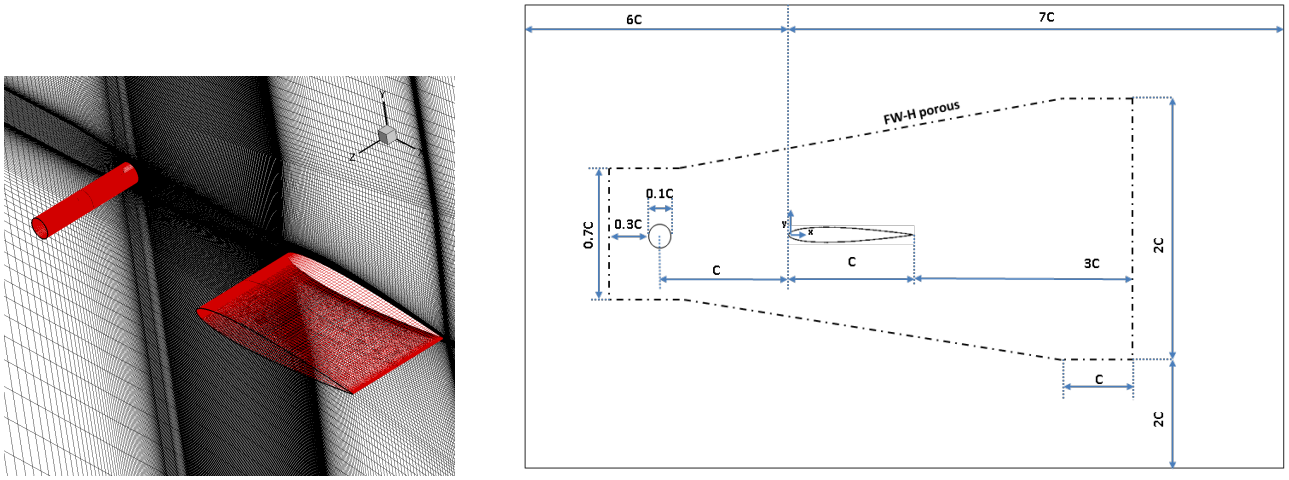

(a) Computational mesh

(b) Computational domain showing location of the porous FWH surface

Figure 2: Computational mesh and sketch of computational domain showing relative dimensions and location of the porous FWH surface

3.5D in the spanwise direction. A symmetric NACA0012 airfoil ($C = 0.1m$) is place one chord-length downstream of the rod ($D = 0.1C$). The flow conditions used are the same as the reference experiment [9]. The incoming velocity is $72m/s$ with a turbulence intensity $Tu = 0.8\%$. The Reynolds number based on the airfoil chord is $Re_C = 4.8 \times 10^5$. The grid consists of 6 million cells with 250 points around the rod, 548 points around the airfoil in the circumferential direction and 65 points in the spanwise direction, as shown on Figure 2(a). The nondimensional wall distance $y^+ \sim 1$ for both the rod and the cylinder. Relative dimensions of the computational domain as well as the location of the porous FWH surface are shown on Figure 2(b).

3.2 Resolution of Near-Field Turbulence

The DDES simulation is run for 25 convective time units (based on the airfoil chord) at a constant time step of $\Delta t = 10^{-6}s$ through the transient phase, after which the flow samples are collected for the computations of the mean flow field and the far-field acoustics. Figure 3 shows instantaneous vorticity iso-surfaces from the sampling window – the resolved turbulent structures and the breakdown in the wake of the rod are clearly visible. The mean streamwise velocity profiles at $x = -0.255D$ (between the rod and the airfoil) and $x = 1.10D$ (in the wake of the airfoil) appear to be in good agreement with the hot wire anemometry data from the reference experiment and the LES result by Giret et al. [15], as shown on Figure 4.

3.3 Far-Field Acoustic Results

The far-field acoustic pressure is computed using 28,500 samples, corresponding to 38 rod shedding cycles, at three microphone positions located 1.85m from the airfoil mid-chord on the mid-span plane, at angles $45°$, $90°$ and $135°$ to the downstream direction. The far-field narrow band spectra for each observer is obtained by applying standard signal processing tools. We first apply the Hanning window to the signal and then average the FFT of 8 sub-samples with approximately 17000 points, which leads to a spectral resolution of 60Hz.

Figure 5 compares the sound pressure levels of the current result with the reference experiment and the LES result by Peth et al. [13]. At all three angles, the peak SPL and its frequency are in excellent agreement with the experimental data – even better than LES results. The spectral broadening around the peak due to the impingement of the turbulent wake on the airfoil leading edge has also been well captured. The discrepancy at low frequencies may be due to the installation effects in the experiment

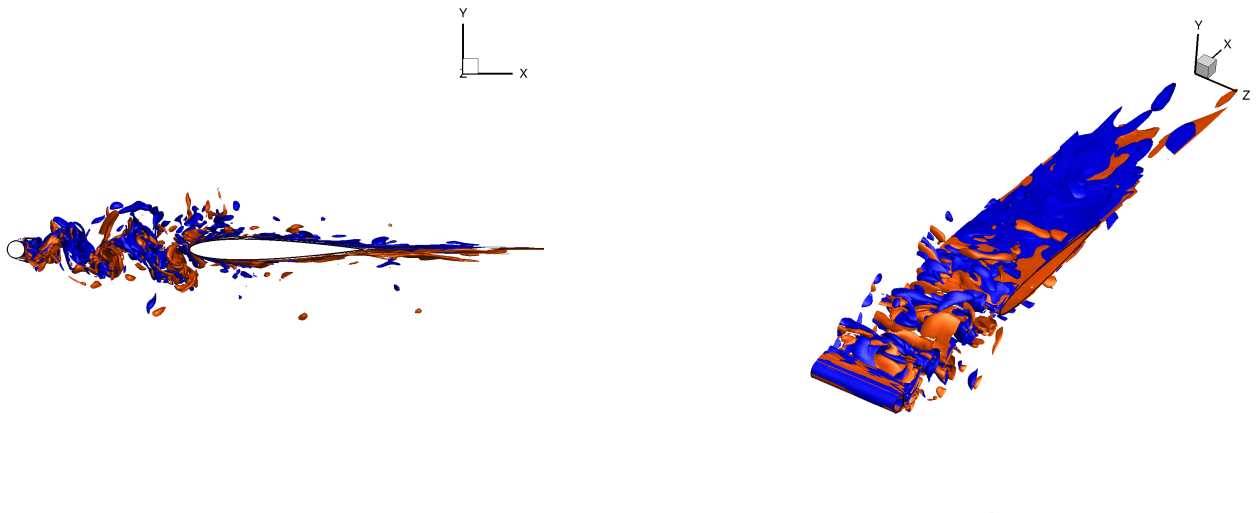

(a) (b)

Figure 3: Instantaneous vorticity iso-surfaces at $\omega_z D/u_\infty = \pm 1$

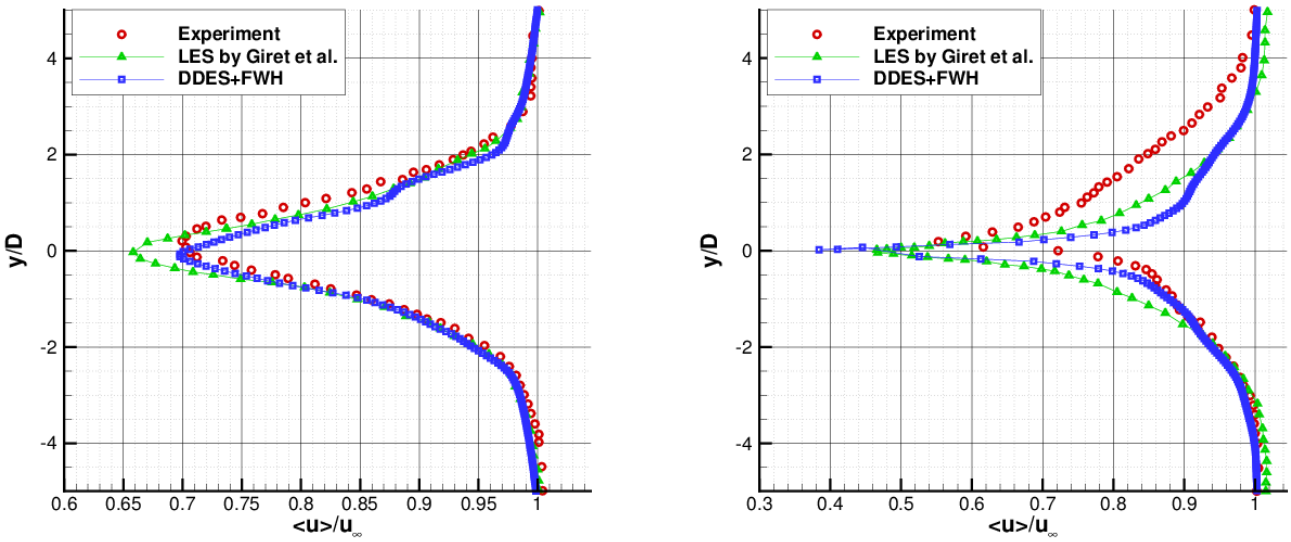

(a) Mean velocity profile at $x = -0.255D$ (b) Mean velocity profile at $x = 1.10D$

Figure 4: Comparison of mean streamwise velocity profile with experiment at $x = -0.255D$ (a) and $x = 1.10D$ (b)

not accounted for in the simulations, as noted by Giret et al. [15]. It is curious that at high frequencies, the SPL is consistently over-predicted at all angles, whereas the LES result by Peth et al. [13] tends to under-predict the same frequency range. The discrepancy may be due to the omission of the quadrupole terms, which were found to have significant impact only on the high frequencies, as noted by Greschner et al. [14].

Figure 6 compares the 3D URANS-based result against experiment and DDES-based result. Acoustic results based on 3D URANS over-predicts the peak SPL by as much as 18dB and the shedding frequency by 20%. This is likely due to the fact that turbulent breakdown in the wake of the rod is not resolved in URANS, causing stronger vortices to impinge on the airfoil leading edge.

3.4 Noise Adjoint Results

To validate the coupled CFD-FWH noise adjoint framework, we compare the noise adjoint against second-order finite difference, on 18 Hicks-Henne surface control points on the airfoil surface (9 on each of the upper and lower surfaces), evaluated over 64 time steps on a 2D slice of the computational

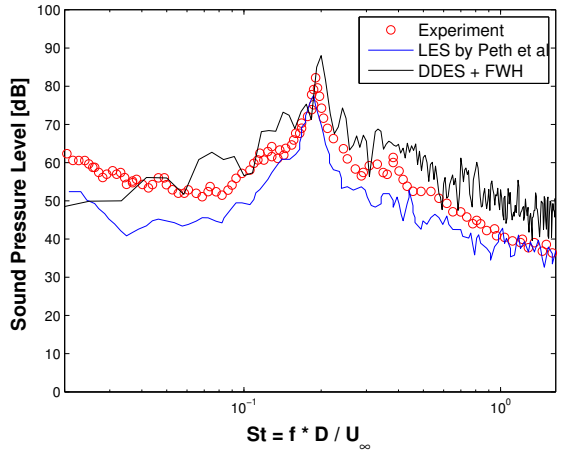

(a) 45°

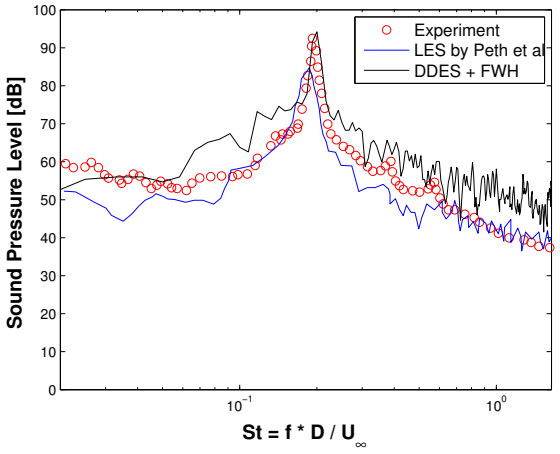

(b) 90°

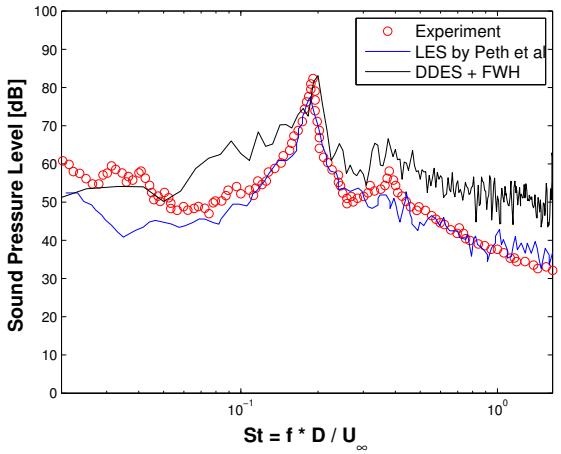

(c) 135°

Figure 5: Comparison of far-field sound spectra with experimental data and LES results from Peth et al. [13]

mesh. A small number of time steps is used because at longer integration times, the accuracy of finite difference deteriorates due to truncation and round-off errors, thus preventing a fair comparison. As shown on Figure 7(a), the agreement for all 18 design variables is excellent.

Having ascertained the accuracy of the noise adjoint, we evaluate it after the convergence of flow statistics over 8 shedding cycles. The noise sensitivity of every surface point in the y-direction is plotted on Figure 7(b). Note that the surface sensitivity smoothly oscillates around zero across the length of the airfoil – the gradient seems to point towards a design with a wavy airfoil profile in order to reduce far-field noise.

4. Conclusion

In this paper, the DDES-FWH noise prediction framework implemented in the open-source multi-physics solver suite SU2 is validated using a benchmark test case the rod-airfoil configuration. The peak sound pressure level and its frequency are in excellent agreement with experimental data. The spectral broadening around the peak is also well captured. The high frequency broadband noise level is over-predicted by the present study, likely due to the omission of the quadrupole contribution that becomes significant in the high frequency range.

In addition, design sensitivities with respect to far-field noise objective function computed based

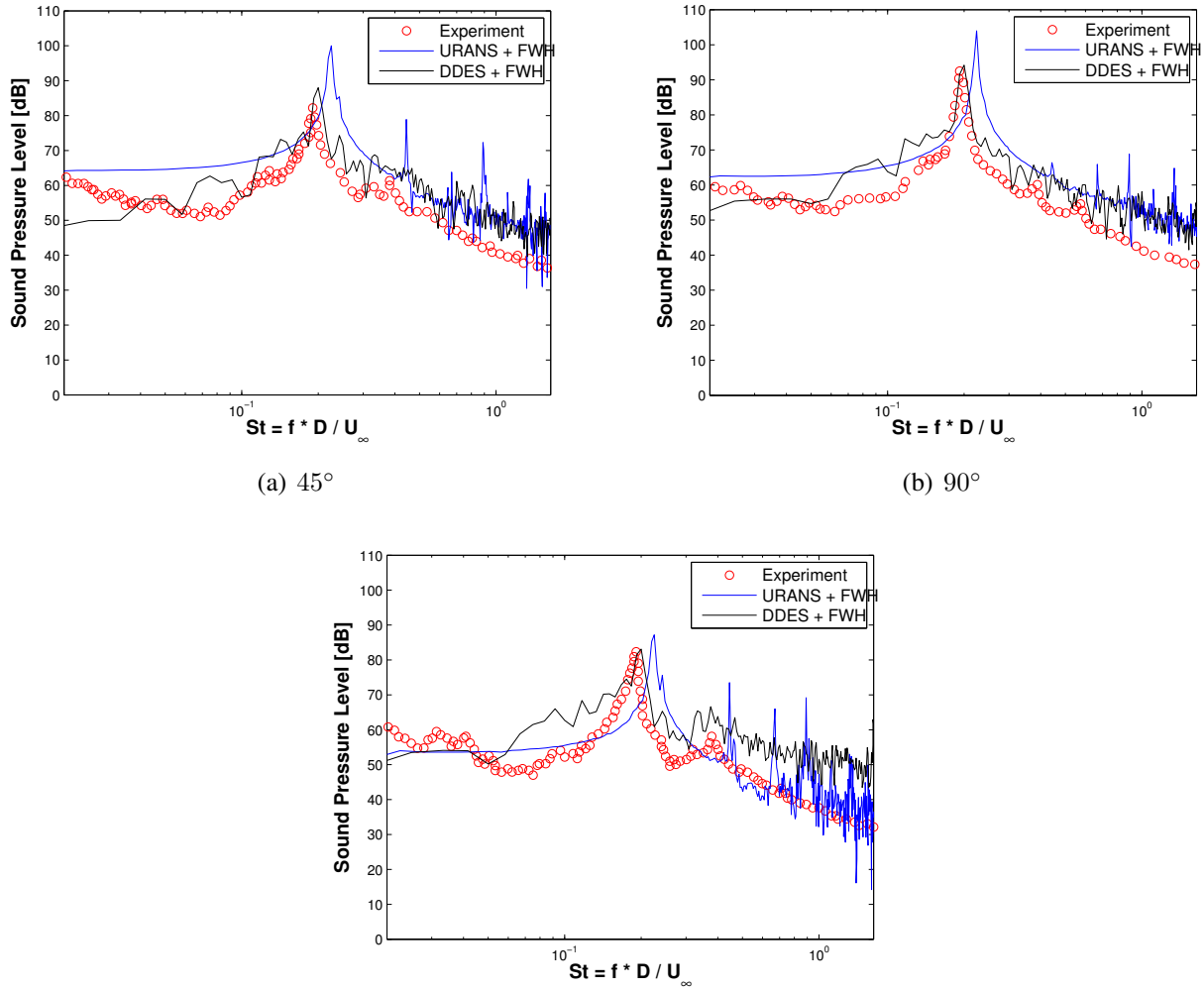

(a) 45°

(b) 90°

(c) 135°

Figure 6: Comparison of far-field sound spectra computed by URANS-FWH and DDES-FWH approaches with experimental data

on a discrete adjoint framework have also been validated against finite difference, thus paving the way to aeroacoustic optimization using high-fidelity simulations in the near future. The noise sensitivity currently points towards a design with a wavy profile for both upper and lower airfoil surfaces in order to reduce far-field noise.

REFERENCES

1. Palacios, F., Economon, T. D., Aranake, A. C., Copeland, S. R., Lonkar, A. K., Lukaczyk, T. W., Manosalvas, D. E., Naik, K. R., Padron, A. S., Tracey, B., Variyar, A., and Alonso, J. J., Stanford University Unstructured (SU2): Open-source analysis and design technology for turbulent flows. *AIAA Paper 2014-0243*, (2014)

2. Jameson, A. Aerodynamic design via control theory. *Journal of Scientific Computing* **3**, 233–260 (1988).

3. Rumpfkeil, M. P. and Zingg, D. W. A hybrid algorithm for far-field noise minimization. *Computers and Fluids* **39**(9), 1516–1528 (2010).

4. Fabiano, E., Mishra, A., Mavriplis, D. and Mani, K. Time-dependent aero-acoustic adjoint-based shape optimization of helicopter rotors in forward flight, *AIAA Paper 2016-1910*, (2016).

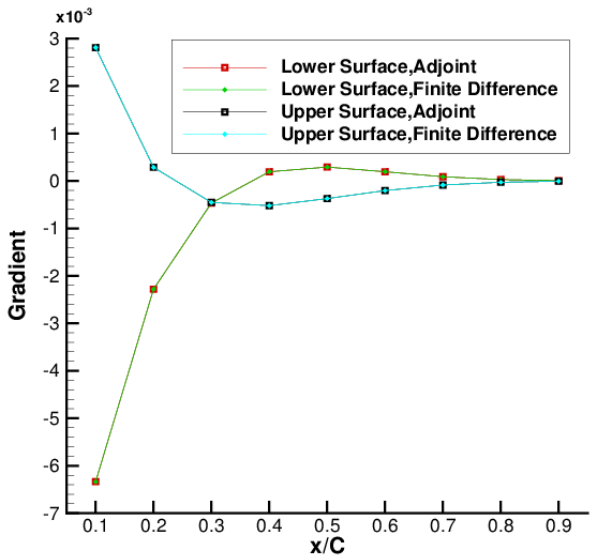

(a) Comparison between adjoint and finite difference gradient values

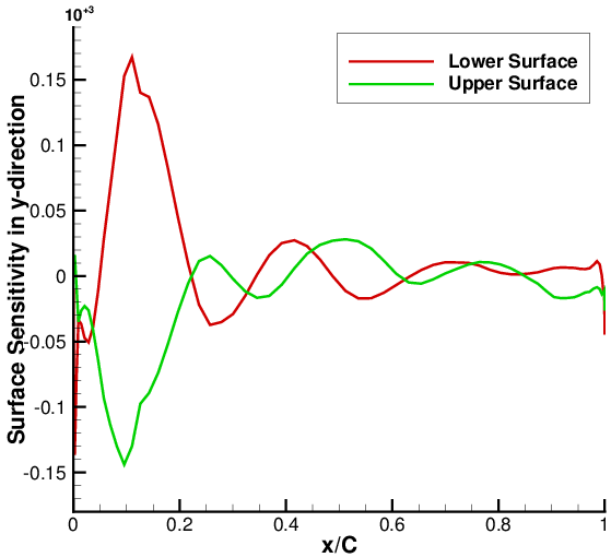

(b) Surface sensitivity in the y-direction evaluated based on 8 shedding cycles

Figure 7: DDES-FWH noise gradient on the airfoil surface based on a 2D slice of computational mesh

5. Zhou, B. Y., Albring, T., Gauger, N. R., Ilario da Silva, C. R., Economon, T. D. and Alonso, J. J. An Efficient Unsteady Aerodynamic and Aeroacoustic Design Framework Using Discrete Adjoint, *17th AIAA/ISSMO Multidisciplinary Analysis and Optimization Conference*,*AIAA Paper 2016-3369*, (2016).

6. Shur M., Spalart P. R., Strelets M., and Travin A. Detached-eddy simulation of an airfoil at high angle of attack, *4th International Symposium of Engineering Turbulence Modelling and Measurements*, (1999).

7. Spalart, P. Strategies for turbulence modelling and simulations, *International Journal of Heat and Fluid Flow*, **21**, (3) 252–263, (2000).

8. Spalart, P., Jou, W., Strelets, M. and Allmaras, S. Comments on the feasibility of LES for wings, and on a hybrid RANS/LES approach, *Advances in DNS/LES*, **1**, 4–8, (1997).

9. Jacob, M. C., Boudet, J., Casalino, D. and Michard, M. A rod-airfoil experiment as benchmark for broad-band noise modeling, *Theoretical and Computational Fluid Dynamics*, **19**, 171–196, (2005).

10. Molina, E. S., Spode, C., da Silva, R. G., Manosalvas-Kjono, D. E., Nimmagadda, S., Economon, T. D., Alonso, J. J. and Righi, M. Hybrid RANS/LES Calculations in SU2, *18th AIAA/ISSMO Multidisciplinary Analysis and Optimization Conference*, (2017).

11. Di Francescantonio, P., A New Boundary Integral Formulation for the Prediction of Sound Radiation. *Journal of Sound and Vibration* **202**(4), 491–509 (1997).

12. Boudet, J., Grosjean, N. and Jacob, M. C. Wake-airfoil interaction as broadband noise source: a large-eddy simulation study, *International Journal of Aeroacoustics*, **4**, 93–116, (2005).

13. Peth, S., Seo, J. H., Moon, Y. J., Jacob, M. C., Thiele, F. Computation of aerodynamic noise from rod wake-airfoil interactions, *European Conference on Computational Fluid Dynamics, ECCOMAS CFD*, (2006).

14. Greschner, B., Thiele, F., Jacob, M., and Casalino, D. Prediction of sound generated by a rod?airfoil configuration using EASM DES and the generalised Lighthill/FW-H analogy, *Computers and Fluids*, **37**, 402–413, (2008).

15. Giret, J., Sengissen, A., Moreau, S., Sanjosé, M. and Jouhaud, J. Prediction of the Sound Generated by a Rod-airfoil Configuration Using a Compressible Unstructured LES Solver and a FW-H Analogy, *Proceedings of the 18th AIAA/CEAS Aeroacoustics Conference*, (2012).